



# Hydrogen Plasma-Assisted Atomic Layer Deposition of Ru with Low Oxygen Content

Geonwoo Park<sup>1</sup> · Keunhoi Kim<sup>1</sup> · Jeong Woo Shin<sup>2,3</sup> · Geongu Han<sup>1</sup> · Dohyun Go<sup>4</sup> · Jihwan An<sup>1,2,5</sup>

Received: 7 August 2023 / Revised: 18 November 2023 / Accepted: 21 November 2023 / Published online: 21 February 2024  
© The Author(s), under exclusive licence to Korean Institute of Chemical Engineers, Seoul, Korea 2024

## Abstract

Ru is extensively used in electrical and energy applications because of its high electrical conductivity and catalytic activity. This study reports the H<sub>2</sub> plasma-enhanced atomic layer deposition (PEALD) of Ru thin films using a novel carbonyl cyclohexadiene ruthenium precursor. The optimized process conditions for depositing Ru thin films by PEALD were established based on the growth per cycle (GPC), chemical formation, crystallinity, conformality, and resistivity, according to process parameters such as precursor pulse time, H<sub>2</sub> plasma pulse time, purge time, and deposition temperature. Pure Ru thin films (low carbon and oxygen) were deposited with low resistivity (30.8 μΩ cm) and showed high conformality (> 95%) on the Si trenches. The oxidant-free PEALD Ru process reported in this study may have implications on the fabrication of high-quality interfaces between Ru and easily-oxidized substrates.

**Keywords** Plasma enhanced atomic layer deposition · Ruthenium · Hydrogen plasma · Electrode · Catalyst

## Introduction

Ru exhibits interesting electrical, electrochemical, and catalytic properties. Moreover, Ru shows a low sheet resistance (7.1 μΩ cm for bulk), high work function (4.7 eV), and low solid solubility in Cu [1]. Moreover, Ru exhibits superior

catalytic activity, for example, in the oxygen/hydrogen evolution reaction (OER/HER) and hydrocarbon/natural gas reforming, and is less expensive than other noble metals (Pt, Pd, and Ir) [2–5]. Therefore, Ru is extensively utilized and studied in various fields such as semiconductors (e.g., electrodes for metal–oxide–semiconductor field-effect transistors (MOSFETs) and dynamic random-access memory (DRAM) capacitors) [6–9], electrochemical devices (e.g., electrolysis and hydrocarbon-fueled solid oxide fuel cells (SOFC)) [10, 11], and catalysts (e.g., carbon capture devices) [12, 13].

Atomic layer deposition (ALD) has been actively studied in various fields owing to its unique advantages. Based on a self-limiting layer-by-layer growth mechanism, ALD enables precise thickness control and highly uniform and conformal thin-film growth on a complex structure [13, 14]. Most Ru ALD processes involve O-containing reactants that can form an unwanted oxide layer on the substrate [15, 16]. For example, when Ru was directly deposited on a Ta or TiN layer, oxide layers such as Ta<sub>2</sub>O<sub>5</sub> or TiO<sub>2</sub> formed [17, 18]. Notably, these interfacial oxide layers exhibit poor electromigration resistance, which can reduce the capacitance in capacitor devices [19]. To address the above-mentioned concerns, previous studies have explored Ru ALD processes that do not use oxidizing reactants [20]. The oxidant-free Ru ALD process aims to enhance the overall performance and reliability of the deposited Ru films by eliminating the

Geonwoo Park and Keunhoi Kim contributed equally to this work.

✉ Dohyun Go  
dogo@ucsd.edu

✉ Jihwan An  
jihwanan@postech.ac.kr

<sup>1</sup> Department of Manufacturing Systems and Design Engineering (MSDE), Seoul National University of Science and Technology, Seoul, Republic of Korea

<sup>2</sup> Energy and Environment Research Institute, Seoul National University of Science and Technology, Seoul, Republic of Korea

<sup>3</sup> Department of Mechanical and Aerospace Engineering, Nanyang Technological University, Singapore, Singapore

<sup>4</sup> Department of Chemistry and Biochemistry, University of California San Diego, 9500 Gilman Dr, La Jolla, CA 92093, USA

<sup>5</sup> Department of Mechanical Engineering, Pohang University of Science and Technology (POSTECH), 77 Cheongam-ro, Nam-gu, Pohang, Gyeongbuk 37673, Republic of Korea

possibility of forming unwanted oxide layers. Consequently, investigating alternative Ru ALD processes is imperative to overcome the limitations associated with oxidizing reactants and facilitate the deposition of high-quality Ru films for various applications.

In this study, a plasma-enhanced atomic layer deposition (PEALD) process for Ru using a novel carbonyl cyclohexadiene ruthenium precursor and hydrogen plasma is demonstrated. Process optimization is conducted based on the growth per cycle (GPC), chemical formation, and crystallinity of the PEALD Ru film using X-ray reflectivity (XRR), X-ray photoelectron spectroscopy (XPS), and grazing-incidence X-ray diffraction (GIXRD). The optimized ALD process conditions for the novel precursor are established in the deposition temperature range of 150–275 °C. The PEALD Ru film exhibited a low impurity content (C: 3.7 at% and O: 0.7 at%) with polycrystalline structure. High conformality of the PEALD Ru film on the three-dimensional (3D) structure (aspect ratio of approximately 1:4) is demonstrated. The PEALD Ru thin film showed a low resistivity (30.8  $\mu\Omega$  cm), which is within the range reported by previous studies based on different combinations of precursors and reactants (10–36  $\mu\Omega$  cm) [21].

## Experimental

### PEALD Ru Deposition

A customized PEALD system with a remote inductively coupled plasma (ICP) source was used. A schematic of the customized remote inductively coupled PEALD system is shown in Fig. S1. Carbonyl cyclohexadiene ruthenium (Air Liquide, France) was used as the Ru precursor, H<sub>2</sub> plasma as the reactant, and Ar gas as the carrier gas. The Ru precursor was evaporated at 45 °C, which is a relatively low temperature for precursor evaporation compared to the existing Ru precursor [22–24]. H<sub>2</sub> plasma was generated at 900 mTorr with a radio-frequency (RF) power of 150 W. The PEALD Ru deposition conditions were optimized by changing: (1) precursor pulse time (0.5, 1, and 2 s), (2) H<sub>2</sub> plasma pulse time (5, 10, and 20 s), and (3) purge time (15, 30, and 60 s). In addition, the deposition temperature was adjusted to 150, 200, 250, and 275 °C to determine the ALD window. The conformality of PEALD Ru was evaluated on a trench structure with an aspect ratio of 1:4 (~3  $\mu$ m hole diameter and ~12  $\mu$ m depth) according to the following sequence: 1 s precursor pulse, 10 s exposure, purge 30 s, H<sub>2</sub> plasma pulse 10 s, and purge 30 s.

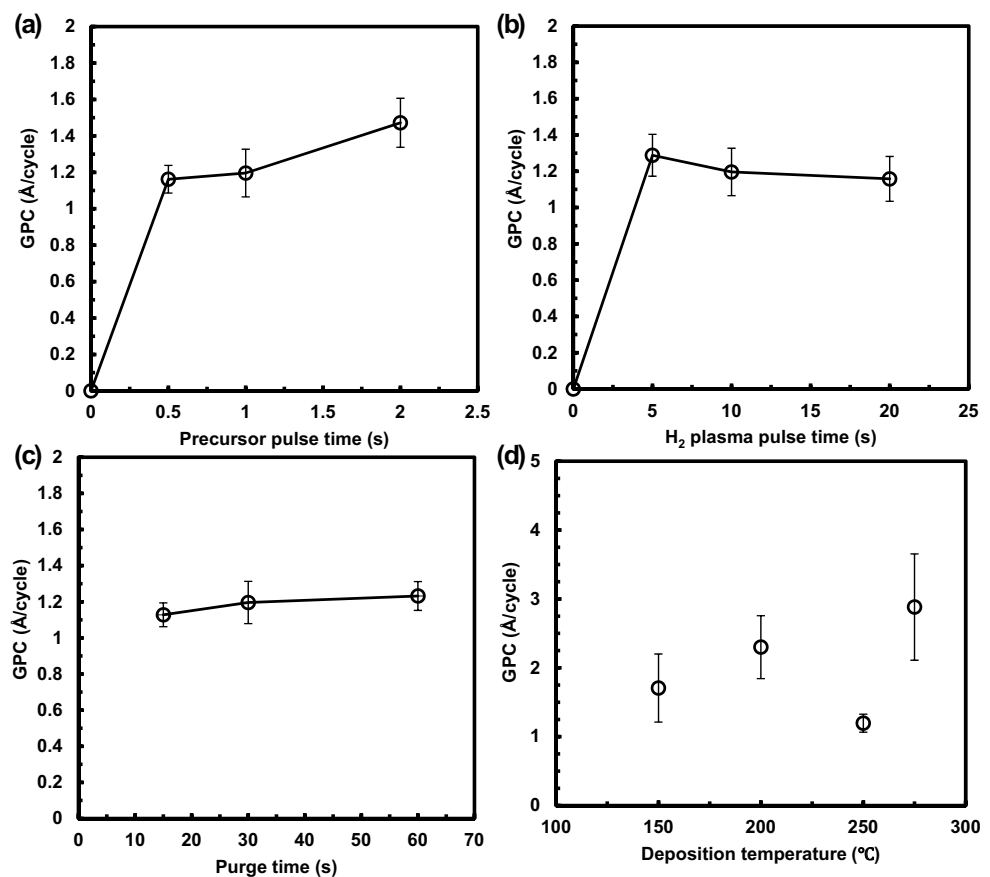
## Structural and Electrical Characterization

The surface morphologies of the PEALD Ru thin films were analyzed by high-resolution field-emission scanning electron microscopy (HR-FESEM; SU8010, Hitachi High Technologies Corporation). The thicknesses and densities of the PEALD Ru thin films were analyzed by XRR (SmartLab, Rigaku Corporation) using Cu-K $\alpha$  radiation at a wavelength of 1.54 Å from 0.0° to 5.0° with a 0.0012° step size. The crystallinity of the PEALD Ru was evaluated by GIXRD in the 2theta range of 10°–90° using the same equipment as used for the XRR measurements. Compositional analysis was performed by XPS (K-Alpha+, Thermo Fisher Scientific Corporation) using an Al-K $\alpha$  source gun after etching using 1 keV Ar ions to eliminate surface contamination. The Ru thin film was deposited on a quartz substrate to measure its resistivity. The resistivity of the PEALD Ru was calculated as  $\rho = R/d$ , where  $\rho$  is the resistivity,  $R$  is the sheet resistance, and  $d$  is the PEALD Ru film thickness (calculated by GPC: 0.12 nm/cycle). The sheet resistance was measured using a four-point probe (CMT-SR2000, Changmin Tech Corporation), and the thickness was measured using XRR.

## Results and Discussion

To optimize the ALD process, a comprehensive study of process parameters including: (1) precursor pulse time (0.5, 1, and 2 s), (2) H<sub>2</sub> plasma pulse time (5, 10, and 20 s), (3) purge time after precursor/H<sub>2</sub> plasma pulse (15, 30, and 60 s), and (4) deposition temperature (150, 200, 250, and 275 °C), as shown in Fig. 1. The XRR results of the film thicknesses as functions of the pulse time, H<sub>2</sub> plasma pulse time, and purge time after the precursor/H<sub>2</sub> plasma pulse are shown in Fig. S2, and the results are summarized in Table S1. As shown in Fig. 1a–c and Table S1, the carbonyl cyclohexadiene ruthenium precursor showed a constant GPC independent of the precursor pulse time, H<sub>2</sub> plasma pulse time, and purge time after the precursor/H<sub>2</sub> plasma pulse, which is a well-known deposition characteristic of ALD based on self-limiting growth behavior. In contrast, the carbonyl cyclohexadiene ruthenium precursor is highly sensitive to the deposition temperature. The GPC at 250 °C is stable and shows high uniformity independent of the deposition location, whereas the GPC at 150, 200, and 275 °C is higher than that at 250 °C and exhibits significant fluctuations depending on the deposition location, as shown in Fig. 1d and Table S1. The higher GPC and significant fluctuations in the deposition thickness may be due to the insufficient thermal energy to complete surface

**Fig. 1** PEALD Ru process parameter investigation on **a** precursor pulse time (0.5, 1, and 2 s), **b** H<sub>2</sub> plasma pulse time (5, 10, and 20 s), **c** purge time after precursor/H<sub>2</sub> plasma pulse (10, 30, and 60 s), and **d** deposition temperature (150, 200, 250, and 275 °C)



reactions at low temperatures and the possible decomposition of surface species with additional reactant adsorption at high temperatures [25]. Thus, it is plausible that an ALD window exists within a limited temperature range close to 250 °C.

Based on the results presented in Fig. 1 and Table S1, the standard process condition for PEALD Ru was established: 1 s Ru precursor pulse, 10 s exposure time, 30 s Ar purge time, 10 s H<sub>2</sub> plasma pulse time, and 30 s Ar purge time at a temperature of 250 °C. The thicknesses of the PEALD Ru films, as a function of the number of ALD cycles, was investigated, as shown in Fig. 2a and b. The PEALD Ru films prepared by 50, 100, and 200 cycles exhibited thicknesses of  $7.3 \pm \sim 0.2$ ,  $13.4 \pm \sim 0.2$ , and  $34.3 \pm \sim 0.3$  nm, respectively. The thickness of PEALD Ru increased linearly with the number of ALD cycles, which is a well-known self-limiting ALD growth characteristic. XPS and XRD analyses were conducted to investigate the film purity and crystallinity of PEALD Ru. Figure 2c shows the high-resolution XPS spectra of the Ru 3*d* and C 1*s* peaks of the PEALD Ru films based on the XPS survey scan results (Fig. S3). The Ru 3*d* and C 1*s* peaks were deconvoluted for carbon analysis because of the binding energy overlap between Ru 3*d* and C 1*s*. The detailed data for the fitted single components are

summarized in Table S2. PEALD Ru contained 95.54 at% Ru, 3.71 at% C, and 0.74 at% O, indicating that the PEALD Ru prepared using the carbonyl cyclohexadiene ruthenium precursor has low carbon and oxygen impurities. Figure 2d shows the GIXRD results, which indicate that the PEALD Ru film is polycrystalline, and the (002) and (101) orientations of Ru are the most prominent at 38.6° and 44.4°, respectively (from the standard ICDD, PDF Card No.: 00-006-0663).

The conformality of PEALD Ru was evaluated by deposition on a ~1:4 aspect ratio trench Si substrate (~3 μm hole diameter and ~12 μm depth) under the optimized process conditions, as shown in Fig. 3. It is recognized that PEALD has relatively low conformality compared with thermal ALD because of the inhibitory effect of the surface recombination of plasma species during the penetration of plasma species into the hole structure [26]. However, conformal deposition via PEALD on 3D structure can be achieved by increasing radical flux through high plasma power, extended plasma pulse time, closely spaced plasma source and substrate, etc. [26, 27]. In this PEALD Ru process, we successfully deposit conformal Ru thin film on a ~1:4 aspect ratio trench substrate by increasing H<sub>2</sub> plasma pulse time. Plasma species that were not recombined with the substrate entered

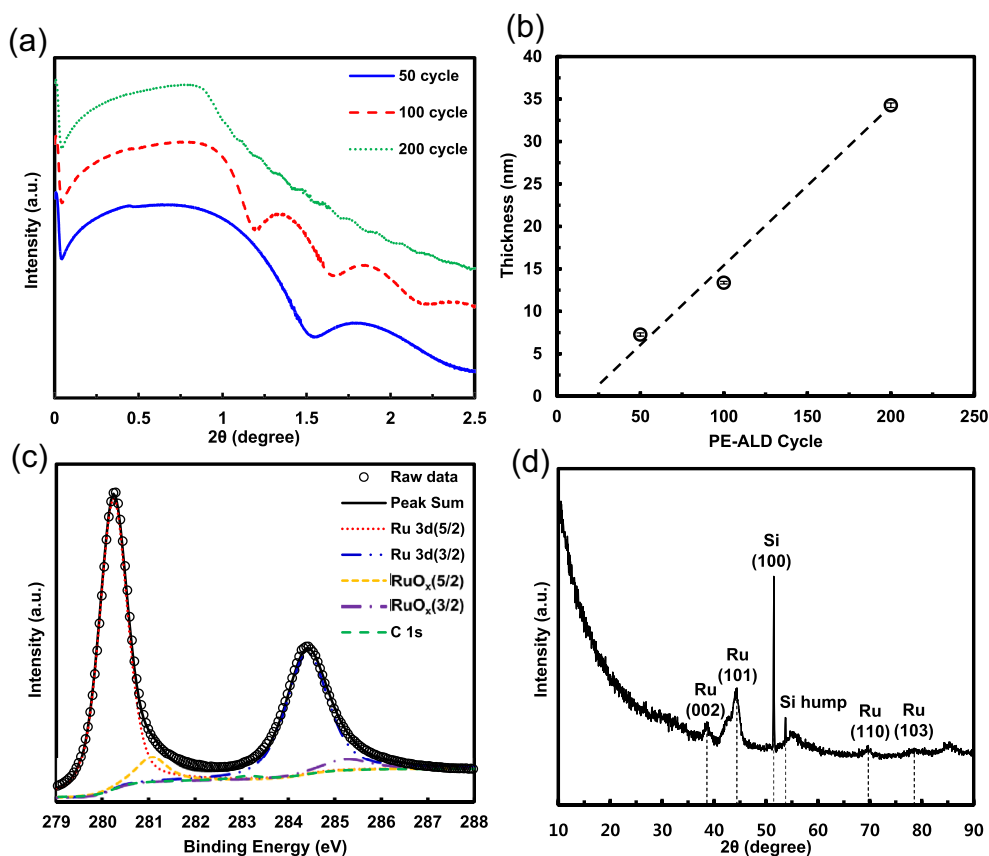


**Fig. 2** **a** XRR results of the PEALD Ru prepared by 50, 100, and 200 cycles, **b** the fitted thicknesses determined by XRR, **c** high-resolution XPS spectra of Ru 3d peak, and **d** GIXRD of the PEALD Ru film with a thickness of 9.4 nm

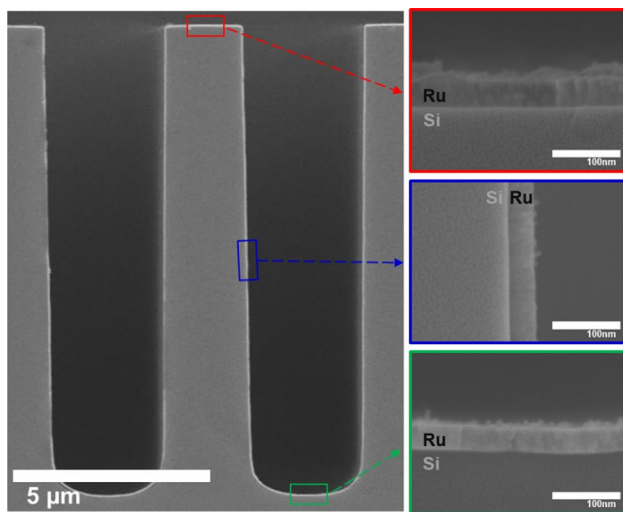
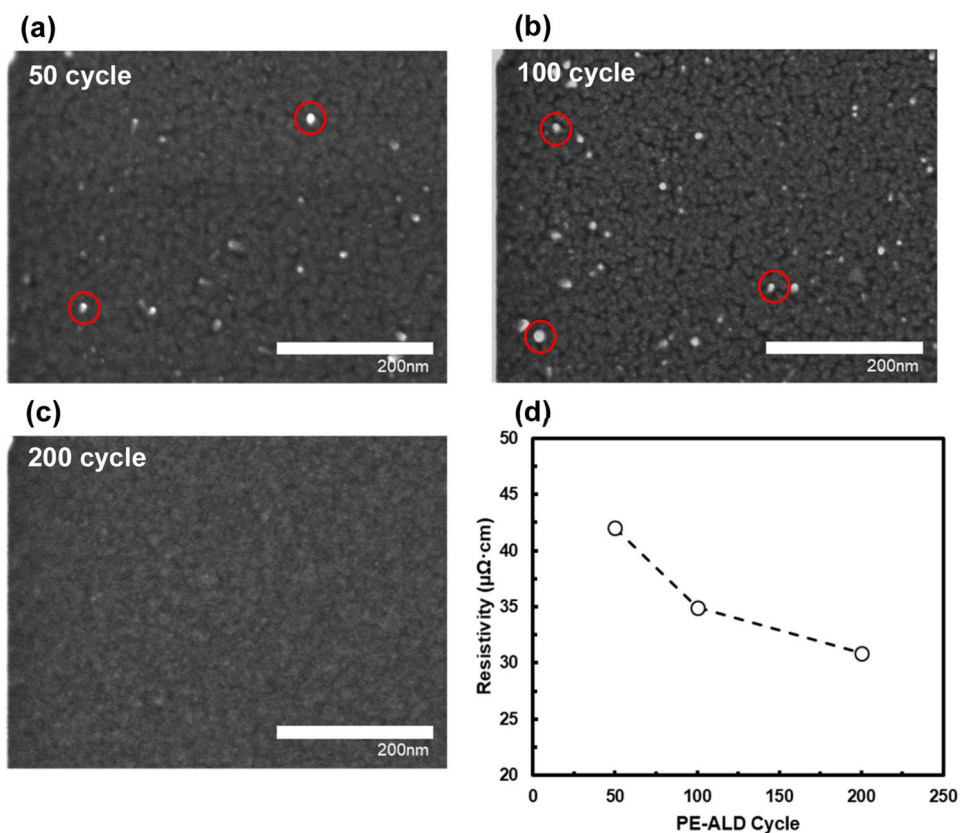


**Fig. 3** HR-SEM image of the PEALD Ru thin film deposited on a 3D trench Si substrate with a  $\sim 1:4$  aspect ratio ( $\sim 3 \mu\text{m}$  hole diameter and  $\sim 12 \mu\text{m}$  depth)

well into the bottom of the hole structure, which is due to the increased radical densities that allow overcoming surface recombination. As a result, the Ru thin film exhibited a thickness of 39 nm at the top surface, 38.7 nm at the mid-surface, and 35.7 nm at the bottom surface. These results indicated conformal deposition with a thickness difference of approximately 5% between the top and bottom surfaces.

Figure 4 shows the morphologies of the ALD Ru films, as well as the resistivity and thickness of the films, as a function of the number of ALD cycles. The film morphology and electrical resistivity were characterized using HR-SEM and a four-point probe. From the HR-SEM images, nucleation islands (red circles in Fig. 4a and b) remained on the ALD Ru film surface after 50 and 100 cycles, which is attributed to island growth instead of ideal layer-by-layer growth during the initial nucleation stage [28, 29]. In contrast, a smooth full-film of metallic Ru without nucleation islands was observed after 200 ALD cycles, as shown in Fig. 4c. The electrical properties of the Ru thin films were characterized based on the morphological analysis. Relatively high resistivities (42.0 and 34.9  $\mu\Omega \text{ cm}$ ) were measured after 50 and 100 cycles owing to the noncontinuous film morphology. However, the Ru film prepared by 200 cycles has low

**Fig. 4** HR-SEM images of the Ru thin film prepared with different PEALD cycles: **a** 50, **b** 100, and **c** 200. **d** Resistivity of the Ru thin film as a function of PEALD cycles (red circles: nucleation islands)



resistivity (30.8  $\mu\Omega\cdot\text{cm}$ ) and a dense morphology, as shown in Fig. 4c and d. Electrical resistivity is known to be influenced by scattering effects at the surface, interface, and grain boundaries of thin films, and these scattering effects can become dominant with decreasing film thickness [30]. In addition, the thin film density is considered a key factor affecting the resistivity [31]. Consequently, the optimized Ru thin film, deposited using carbonyl cyclohexadiene ruthenium and  $\text{H}_2$  plasma by PEALD, exhibits a resistivity of 30.8  $\mu\Omega\cdot\text{cm}$ , which is comparable with the range of resistivity values reported in previous studies using different combinations of precursors and reactants (10–36  $\mu\Omega\cdot\text{cm}$ ) [21].

## Conclusions

This study demonstrates the first successful PEALD process using a novel precursor, carbonyl cyclohexadiene ruthenium, and  $\text{H}_2$  plasma for the deposition of high-quality Ru thin films. By optimizing the process parameters based on the GPC, chemical formation, crystallinity, conformality, and resistivity, a standard ALD process condition was established. The optimized process conditions yielded a high GPC of approximately 0.12 nm/cycle and a low resistivity of 30.8  $\mu\Omega\cdot\text{cm}$ , making it applicable to

various applications. The deposited films were pure polycrystalline Ru thin films with low levels of carbon and oxygen impurities. In addition, the results of this study showed high conformality in the 3D structures, making the developed method a promising approach for the deposition of Ru thin films with complex geometries. In summary, this study provides valuable insights into the use of PEALD to deposit high-quality Ru thin films for various applications.

**Supplementary Information** The online version contains supplementary material available at <https://doi.org/10.1007/s11814-024-00035-2>.

**Acknowledgements** This work was supported by the National Research Foundation of Korea (NRF) grant funded by the Korea government (MSIT) (No. 20220R1A2C4001205), Basic Science Research Program through the National Research Foundation of Korea (NRF) funded by the Ministry of Education (NRF-2021R1A6A1A03039981), the Technology Innovation Program (No. 20010630) funded by the Ministry of Trade, Industry and Energy (MOTIE) of Korea, and Samsung Electronics Co., Ltd (IO230414-05954-01). The carbonyl cyclohexadiene ruthenium precursor was provided by Air Liquide.

**Data Availability** The data that support the findings of this study are available from the corresponding author upon reasonable request.

## Declarations

**Conflict of interest** The authors declare no conflict of interest.



## References

1. N. Torazawa, T. Hinomura, S. Hirao, E. Kobori, H. Korogi, S. Matsumoto, *ECS J. Solid State Sci. Technol.* **5**, P433 (2016)
2. J. Yu, Q. He, G. Yang, W. Zhou, Z. Shao, M. Ni, *ACS Catal.* **9**, 9973–10011 (2019)
3. S. Kye, H.J. Kim, D. Go, B.C. Yang, J.W. Shin, S. Lee, J. An, *ACS Catal.* **11**, 3523–3529 (2021)
4. S. Cwik, K.N. Woods, M.J. Saly, T.J. Knisley, C.H. Winter, *J. Vac. Sci. Technol. A* **38**, 012402 (2020)
5. A. Rogozhin, A. Miakonkikh, E. Smirnova, A. Lomov, S. Simakin, K. Rudenko, *Coatings* **11**, 117 (2021)
6. J.A. Kittl, K. Opsomer, M. Popovici, N. Menou, B. Kaczer, X.P. Wang, C. Adelman, M.A. Pawlak, K. Tomida, A. Rothschild, *Microelectron. Eng.* **86**, 1789–1795 (2009)
7. V. Misra, G. Lucovsky, G. Parsons, *MRS Bull.* **27**, 212–216 (2002)
8. S.K. Kim, W.-D. Kim, K.-M. Kim, C.S. Hwang, J. Jeong, *Appl. Phys. Lett.* **85**, 4112–4114 (2004)
9. J.H. Han, S.W. Lee, G.-J. Choi, S.Y. Lee, C.S. Hwang, C. Dussarrat, J. Gatineau, *Chem. Mater.* **21**, 207–209 (2009)
10. H.J. Kim, M.J. Kil, J. Lee, B.C. Yang, D. Go, Y. Lim, Y. Kim, *J. An, Appl. Surf. Sci.* **538**, 148105 (2020)
11. D. Go, B.C. Yang, J.W. Shin, H.J. Kim, S. Lee, S. Kye, S. Kim, *J. An, Ceram. Int.* **46**(2), 1705–1710 (2020)
12. H.J. Jeong, J.W. Kim, K. Bae, H. Jung, J.H. Shim, *ACS Catal.* **5**, 1914–1921 (2015)
13. H.J. Jeong, J.W. Kim, D.Y. Jang, J.H. Shim, *J. Power. Sources* **291**, 239–245 (2015)
14. R.L. Puurunen, W. Vandervorst, *J. Appl. Phys.* **96**, 7686–7695 (2004)
15. M. Schaefer, R. Schlaf, *J. Appl. Phys.* **118**, 065306 (2015)
16. S.K. Kim, G. Choi, S.Y. Lee, M. Seo, S.W. Lee, J.H. Han, H. Ahn, S. Han, C.S. Hwang, *Adv. Mater.* **20**, 1429–1435 (2008)
17. Z. Gao, D. Le, A. Khaniya, C.L. Dezelah, J. Woodruff, R.K. Kanjolia, W.E. Kaden, T.S. Rahman, P. Banerjee, *Chem. Mater.* **31**, 1304–1317 (2019)
18. H.-J. Sun, K.-M. Kim, Y. Kim, K.-J. Cho, K.-S. Park, J.-M. Lee, J.-S. Roh, *Jpn. J. Appl. Phys.* **42**, 582 (2003)
19. T.E. Hong, K.-Y. Mun, S.-K. Choi, J.-Y. Park, S.-H. Kim, T. Cheon, W.K. Kim, B.-Y. Lim, S. Kim, *Thin Solid Films* **520**, 6100–6105 (2012)
20. J. Swerts, A. Delabie, M.M. Salimullah, M. Popovici, M.-S. Kim, M. Schaeckers, S. Van Elshocht, *Electrochem. Solid-State Lett.* **1**, P19 (2012)
21. Y. Kotsugi, S. Han, Y. Kim, T. Cheon, D.K. Nandi, R. Ramesh, N. Yu, K. Son, T. Tsugawa, S. Ohtake, R. Harada, Y. Park, B. Shong, S. Kim, *Chem. Mater.* **33**(14), 5639–5651 (2021)
22. C.T. Nguyen, J. Yoon, R. Khan, B. Shong, *Appl. Surf. Sci.* **488**, 896–902 (2019)
23. E.C. Ko, J.Y. Kim, H. Rhee, K.M. Kim, J.H. Han, *Mater. Sci. Semicond.* **156**, 107258 (2023)
24. S.H. Oh, J.M. Hwang, H. Park, D. Park, Y.E. Song, E.C. Ko, T.J. Park, T. Eom, T.M. Chung, *Adv. Mater. Interfaces* **10**, 2202445 (2023)
25. S.M. George, *Chem. Rev.* **110**, 111–131 (2010)
26. M. Kariniemi, J. Niinistö, M. Vehkamäki, M. Kemell, M. Ritala, M. Leskelä, M. Putkonen, *J. Vac. Sci. Technol. A* **30**, 01A115 (2012)
27. J. Dendooven, D. Deduytche, J. Musschoot, R.L. Vanmeirhaeghe, C. Detavernier, *J. Electrochem. Soc.* **157**, G111 (2010)
28. S. Novak, B. Lee, X. Yang, V. Misra, *J. Electrochem. Soc.* **157**, H589 (2010)
29. C. de Paula, N.E. Richey, L. Zeng, S.F. Bent, *Chem. Mater.* **32**, 315–325 (2019)
30. W.-J. Lee, E.-Y. Yun, S.W. Hong, S.-H. Kwon, *Appl. Surf. Sci.* **519**, 146215 (2020)
31. J.W. Shin, J. Lee, K. Kim, C. Kwon, Y. Bin Park, H. Park, K. Kim, H.S. Ahn, D. Shim, *J. An, Ceram. Int.* **48**, 25651–25655 (2022)

**Publisher's Note** Springer Nature remains neutral with regard to jurisdictional claims in published maps and institutional affiliations.

Springer Nature or its licensor (e.g. a society or other partner) holds exclusive rights to this article under a publishing agreement with the author(s) or other rightsholder(s); author self-archiving of the accepted manuscript version of this article is solely governed by the terms of such publishing agreement and applicable law.